Structure of the Calcium Ion-Bound γ-Carboxyglutamic Acid-Rich Domain of Factor IX[†,||]

Steven J. Freedman,[‡,§] Barbara C. Furie,[‡,§] Bruce Furie,[‡,§] and James D. Baleja*[,§]

Center for Hemostasis and Thrombosis Research, Division of Hematology-Oncology, New England Medical Center, and Departments of Medicine and Biochemistry, Tufts University School of Medicine and Sackler School of Graduate Biomedical Sciences, Boston, Massachusetts 02111

Received April 24, 1995; Revised Manuscript Received June 28, 1995[⊗]

ABSTRACT: We have determined the Ca(II)-bound structure of factor IX, residues 1−47, by nuclear magnetic resonance (NMR) spectroscopy. The amino-terminal 47 residues include the γ-carboxyglutamic acid-rich and aromatic amino acid stack domains, and this region is responsible for Ca(II)-dependent phospholipid binding in factor IX. Protons in the 1−47 amino acid sequence were assigned using standard two-dimensional homonuclear NMR experiments. A total of 851 distance restraints and 57 torsion angle restraints were used to generate 17 final structures by distance geometry and simulated annealing methods. The backbone RMSD to the geometric average is 0.6 ± 0.1 Å. The Ca(II)-bound structure is substantially more ordered with increased helical content compared to the apo-factor IX (1−47) structure. The global fold is similar to the crystal structure of the Ca(II)-bound Gla domain of prothrombin fragment I from residues 12 to 47 (RMSD ~1.3 Å), but the backbone conformation differs in the first 11 residues, particularly between residues 3 and 6. The amino-terminal nine Gla residues are oriented to the interior of the protein and suggest an internal Ca(II) binding pocket. The carboxyl-terminal three Gla residues are exposed to solvent. The majority of hydrophobic residues are required to stabilize a globular core in the carboxyl-terminal three-quarters of the molecule. However, a hydrophobic surface patch in the amino-terminal region may represent a phospholipid binding site in factor IX.

Factor IX, a member of the vitamin K-dependent protein family, plays a central role in blood coagulation. This is exemplified by the bleeding disorder hemophilia B, where factor IX activity is deficient. The phospholipid binding activity of factor IX and the other vitamin K-dependent blood coagulation proteins is critical for their proper biological function (Furie & Furie, 1988). The activation of vitamin K-dependent zymogens and the catalytic activity of their activated forms are maximal when they interact with phospholipid membranes in a Ca(II)-dependent manner. The amino-terminal Gla[1] domain is responsible for Ca(II) and phospholipid binding (Furie & Furie, 1988). Specifically, these functions require the presence of 9−12 γ-carboxyglutamic acid (Gla) residues in vitamin K-dependent proteins. Although Gla domains can bind a variety of divalent metal ions other than Ca(II), only Ca(II) supports phospholipid binding (Nelsestuen et al., 1976).

The Gla residues directly participate in Ca(II) binding via their malonate-like side chains. There are several classes of Ca(II) binding sites in Gla domains, some of which interact with Ca(II) in a positively cooperative manner (Strickland & Castellino, 1980; Bajaj, 1982; Nelsestuen & Suttie, 1972; Furie & Furie, 1975; Amphlett et al., 1981). The Gla composition of these sites has been revealed from the seven Ca(II)−coordination complexes in the prothrombin fragment 1 crystal structure (Soriano-Garcia et al., 1992). The anionic Gla residues face the protein interior to form an intricate network of binding sites of varying geometry. Most of the calcium ions are liganded by three or more Gla residues.

The vitamin K-dependent proteins undergo two sequential conformational transitions following their interaction with metal ions (Borowski et al., 1986; Liebman et al., 1987). The first transition is not specific for the divalent metal ion and has been monitored by fluorescence quenching, circular dichroism, and conformation-specific antibodies (Nelsestuen, 1976; Bloom & Mann, 1978; Furie et al., 1978; Borowski et al. 1986). Calcium ions can induce the second conformational transition that leads to phospholipid binding; this structure can also be detected with conformation-specific antibodies (Borowski et al., 1986; Liebman et al., 1987). The Ca(II)-induced structural transition is from a relatively disordered Gla domain to a well-ordered, compact structure (Soriano-Garcia, 1992; Vysotchin et al., 1993; Freedman et al., 1995). We have previously identified three segments of secondary structure separated by the relatively unstructured

[†] This work was performed by S.J.F. in partial fulfillment of the requirements for the degree of Doctor of Philosophy from Tufts University. This work was supported by a grant (HL42443) from the National Institutes of Health. The NMR spectrometer was acquired with a grant (RR06282) from the National Institutes of Health.

[||] The factor IX (1−47)−Ca(II) structure has been deposited in the Brookhaven Protein Data Bank under file name 1CFI. Distance and torsion angle restraints, including force constants, and the molecular topology file are also available.

* Corresponding author [telephone, (617) 636-6872; telefax, (617) 636-6409].

[‡] New England Medical Center and Department of Medicine, Tufts University School of Medicine and Sackler School of Graduate Biomedical Sciences.

[§] Department of Biochemistry, Tufts University School of Medicine and Sackler School of Graduate Biomedical Sciences.

[⊗] Abstract published in *Advance ACS Abstracts,* September 1, 1995.

[1] Abbreviations: γ or Gla, γ-carboxyglutamic acid; NMR, nuclear magnetic resonance; NOE, nuclear Overhauser effect; NOESY, NOE spectroscopy; TOCSY, total correlation spectroscopy; DQF-COSY, double-quantum-filtered correlation spectroscopy; TPPI, time-proportional phase incrementation; RMSD, root-mean-square deviation; GnHCl, guanidine hydrochloride.

0006-2960/95/0434-12126$09.00/0

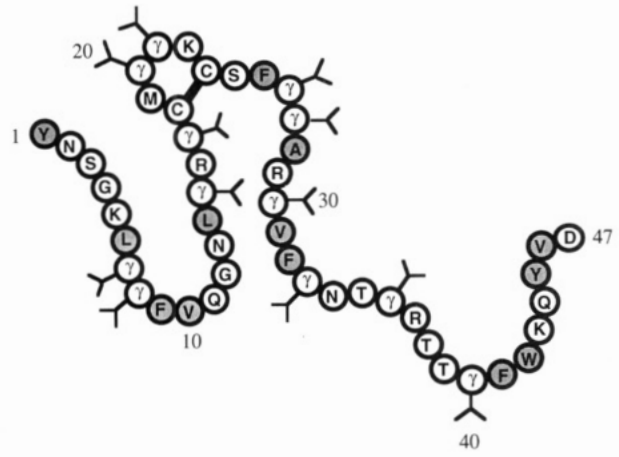

FIGURE 1: Amino acid sequence of the factor IX (1−47) peptide. The Gla domain consists of residues 1−38, and the aromatic amino acid stack domain consists of residues 39−46. An extra amino acid, Asp 47, which corresponds to the first amino acid of the first epidermal growth factor domain of factor IX, was included for purposes of chemical synthesis. The 12 Gla residues are represented by the symbol γ; the Y structures represent the carboxylate groups. The hydrophobic residues are shaded. The single disulfide bond in this peptide is shown as a thick black bar joining Cys 18 to Cys 23.

peptide backbone in the apo-factor IX Gla domain by nuclear magnetic resonance (Freedman et al., 1995). These three structured regions are conserved in the prothrombin fragment 1−Ca(II) crystal structure, but the Ca(II)-bound prothrombin Gla domain folds into a higher order structure. From the prothrombin fragment 1 crystal structure (Soriano-Garcia et al., 1992), three or four of the seven Ca(II) are buried in the protein and thus likely dictate the folding of this domain. The other Ca(II) are partially solvent-exposed. Two independent models have been proposed to account for the phospholipid binding mechanism of Gla domains. One model proposes that calcium ions bridge negatively charged Gla residues in the protein with negatively charged phosphate groups in the phospholipids (Nelsestuen, 1976). The other model proposes that Ca(II) induces the formation of a phospholipid binding structural determinant (Borowski et al., 1986). Presently, the actual phospholipid binding interaction has not been elucidated but may involve features of both models. In this regard, both ionic and hydrophobic interactions have been found to contribute to the phospholipid binding energy of vitamin K-dependent proteins (Atkins & Ganz, 1992). Recently, mutation of the conserved Leu 5 residue in the homologous protein, protein C (Leu 6 in Factor IX), has been found to disrupt this interaction (Zhang & Castellino, 1994).

We have previously used the factor IX (residues 1−47) peptide as a model for the phospholipid binding structure of factor IX. The sequence of factor IX (1−47) is shown in Figure 1. We now report the three-dimensional structure of the Ca(II)-bound peptide in solution as determined by NMR methods. A comparison of this structure with apo-factor IX (1−47) reveals the nature of the Ca(II)-induced conformational transition in factor IX.

MATERIALS AND METHODS

The synthesis, folding, and purification of the factor IX (1−47) peptide have been previously described (Jacobs et al., 1994; Freedman et al., 1995). NMR spectroscopy was performed on H_2O samples composed of 1.5−2.1 mM peptide, 60 equiv of $CaCl_2$, 3 M urea, 2.5 M guanidine hydrochloride, and 0.5 M deuterated (d_4) acetate, pH 5.2−5.4. This solvent is required to maintain the Ca(II)−peptide complex in solution. The sample also contained 10% D_2O for the deuterium lock signal. For a 1.5 mM peptide sample in D_2O, all reagents were lyophilized from D_2O and then redissolved in 99.96% D_2O. Spectra were collected on a Bruker AMX-500 spectrometer with a proton frequency of 500.14 MHz. The carrier frequency was set on the water resonance, which was suppressed using presaturation. One-dimensional NMR spectra were recorded between 25 and 55 °C to evaluate the stability of the sample and resonance line widths. A one-dimensional spectrum of 0.17 mM peptide, pH 5.9, and 1.25 mM $CaCl_2$ in the absence of solubilizing agents was recorded at 25 °C. The data were acquired with 512 summed scans, 1024 real points, and a spectral width of approximately 7000 Hz. For comparison, a one-dimensional spectrum was recorded on a sample composed of 2.1 mM peptide, 60 equiv of $CaCl_2$, 3 M urea, and 2.5 M guanidine hydrochloride, pH 5.9 at 25 °C. For both samples, Ca(II) binding was shown to be reversible by the addition of the chelating agents EDTA or Chelex 100. The data were acquired with identical parameters to the sample without solubilizing agents, except with 64 summed scans. Both spectra were processed on a Sun SPARCstation 2 using the program Felix (Biosym Technologies, San Diego, CA). The spectra were processed using sine bell window functions shifted by 45° and zero filled to 4096 real points.

Two-dimensional NOESY spectra were recorded with mixing times of 100 ms at 35 °C, and 250 ms at 25, 35, and 45 °C. A total of 2048 real data points were acquired in t_2, 512 TPPI increments in t_1, a spectral width of 7246 Hz in the F_2 dimension, 160 summed scans, and a relaxation delay of 1.3 s between scans. Spectra were multiplied with a squared sine bell window function shifted by 45 °C in t_2 (applied over 1024 points) and a sine bell window function shifted by 60° in t_1 (applied over all 512 points) and zero filled to a 2K by 1K (real) matrix using the Bruker NMR processing program. NOESY cross-peak intensities were converted into three distance classes (strong, 1.7−3.0 Å; medium, 1.7−4.0 Å; weak, 3.0−5.0 Å) and calibrated using published methods (Detlefsen et al., 1991; Hyberts et al., 1992). Nonstereospecifically assigned atoms were treated as pseudoatoms and given correction distances according to the guidelines presented in Wüthrich (1986). Distance restraint information was extracted from both the 100 and 250 ms NOESY spectra, but comparison of these spectra was used to control for spin diffusion effects. TOCSY spectra were recorded and processed using identical parameters as the NOESY, except with mixing times of 25, 43, and 60 ms, 96 summed scans, and using an MLEV-17 mixing sequence (Bax & Davis, 1985). A DQF-COSY spectrum was recorded with 2048 real t_2 points and with a spectral width of 7246 Hz, 160 summed scans, and 768 TPPI increments. The spectrum was multiplied by sine bell window functions shifted by 15° in t_2 and 30° in t_1 and zero filled to a 2K by 1K (real) matrix. In addition, NOESY and TOCSY spectra were recorded for the 0.17 mM peptide sample in the absence of solubilizing agents using identical parameters.

Sequence-specific resonance assignments were made in two steps: (1) identification of intraresidue spin systems

using the $^1H-^1H$ through-bond connectivities found in TOCSY and DQF-COSY spectra; (2) sequential assignment of residues on the basis of sequential $d_{\alpha N}$, $d_{\beta N}$, and d_{NN} NOE connectivities (Wüthrich et al., 1982). NOESY spectra were obtained at temperatures between 25 and 45 °C to separate resonances that might be overlapping or to shift resonances bleached out by saturation of the water resonance under one set of conditions but not another. Finally, a NOESY spectrum collected on a sample in D_2O at 35 °C was used to distinguish aromatic from amide protons and expose α protons that were near the presaturated water resonance in H_2O spectra. The NOE contacts from the 100 and 250 ms spectra were then determined using a complete set of proton resonance assignments. The NOE contacts were classified into five categories: (1) "intraresidue" for NOEs within a residue; (2) "sequential" for contacts between the backbone and side-chain protons of residue i with the backbone amide proton of residue $i+1$; (3) "short range" for all other contacts between residue i and $i+1$; (4) "medium range" for NOEs between protons on residues separated by three amino acid positions or less in the sequence; and (5) "long range" for contacts between residues that are separated by four amino acid positions or more in sequence.

The vicinal spin−spin coupling constants $^3J_{HN\alpha}$ were used to calculate ϕ torsion angles (Pardi et al., 1984). The coupling constants were measured from the splitting of amide cross-peaks in a NOESY spectrum that was resolution-enhanced by multiplying with a squared sine bell window function shifted by 30° and applied over 2048 (real) points in t_2. For some residues, ϕ torsion angle constraints excluded the positive ϕ angle region by referring to both the size of the coupling constant and the intensity of NOE cross-peaks for intraresidue $d_{N\alpha}(i,i)$ and sequential $d_{\alpha N}(i,i+1)$ and $d_{NN}(i,i+1)$ (Ludvigsen & Poulsen, 1992). For $^3J_{HN\alpha} > 6$ Hz, the upper and lower limits of the constraints were extended to include all possible ϕ angles.

$\chi 1$ torsion angles and β-methylene proton stereospecific assignments were determined from a measurement of $^3J_{\alpha\beta}$ and a comparison of the βH−NH and αH−βH cross-peak intensities in the NOESY spectra for each stereospecific β proton of AMX and AMX-like residues. Gla residues are of the AMX type since the γ proton is exchangeable and is replaced by a deuterium atom in D_2O. $\chi 1$ torsion angle data for the non-AMX residues were obtained from a measurement of the coupling constant, $^3J_{\alpha\beta}$ (valines and threonines), and an analysis of the αH−βH NOE cross-peak shapes (Hyberts et al., 1987; Driscoll et al., 1989). The coupling constants, $^3J_{\alpha\beta}$, were measured from the splitting of β-proton cross-peaks in a D_2O NOESY spectrum that was resolution-enhanced by multiplying with a squared sine bell window function shifted by 30° and applied over 2048 (real) points in t_2. In this manner, the $\chi 1$ conformations were designated as gauche/trans, trans/gauche, and gauche/gauche for AMX residues, gauche/gauche or non-gauche/gauche for non-AMX residues, and trans or gauche for threonines and valines. Stereospecific assignments of the Gly 12 α protons were determined by comparing the quality and final energies of the structures having the two possible chiralities.

Structure determination used a set of 851 distance restraints (intraresidue and sequential, 424; short, medium, and long range, 427), 19 ϕ angle restraints, 38 $\chi 1$ angle restraints, and stereospecific distance restraints for eight residues. A combination of distance geometry and simulated annealing methods (Havel, 1991) was used to generate 20 converging structures using the DGII program of InsightII (Biosym Technologies, San Diego, CA). The simulated annealing protocol involves an increase in temperature to an upper bound, T_{max}, followed by cooling to zero according to the schedule:

$$T_{max} = T^0_{max}(3x_i^2 - 2x_i^3)$$

The initial upper bound temperature, T^0_{max}, was defined as 200 K. The term x_i refers to the extent of the annealing at the ith step according to $(S_{max} - i)/(S_{max})$, where S_{max} is the total number of steps (20 K). Of the 20 structures calculated, 17 had final total error function values of 1.2 ± 0.1 kcal/mol. Two structures were discarded since they were >2.4 kcal/mol with only small, randomly distributed distance violations (<0.2 Å). Another was discarded since it had a clearly misfolded segment (residues 3−7) that had several distance violations >0.3 Å. An additional round of 20 structures was calculated with the inter-calcium ion distances and distances between liganding Gla residue α, β, and γ carbons and calcium ions as defined by the prothrombin fragment 1 crystal structure (Soriano-Garcia et al., 1992). Average structures were calculated for both ensembles using the Analysis program of InsightII. Average root-mean-square deviation (RMSD) values following superimposition of the backbone atoms of each structure with the geometric average reflected the quality of the structures determined. In addition, the coherence of torsion angles among different structures was evaluated. The average torsion angle was measured by a vector addition method (Hyberts et al., 1992). An order parameter, S, equals 1.0 when the torsion angle is the same in all structures, whereas an order parameter near 0 indicates disorder. Since hydrogen-bonding restraints were not employed in the structure calculations, a hydrogen-bonding analysis was performed on the ensemble of structures using the InsightII program. Hydrogen bonds were defined by a distance less than 2.5 Å between the donor proton and heavy atom acceptor and by an angle between 120° and 180° of the heavy atom donor, proton, and heavy atom acceptor. A hydrogen bond was said to occur if it was present in greater than 70% of the structures.

RESULTS

To determine the structure of the phospholipid binding region of factor IX, we have performed ^1H NMR studies on an amino-terminal 47-residue peptide of factor IX complexed to Ca(II). Factor IX (1−47) in the presence of calcium ions binds to phospholipid vesicles (Jacobs et al., 1994). One-dimensional ^1H NMR spectra in aqueous solution indicate that the factor IX (1−47)−Ca(II) binary complex is well ordered on the basis of the dispersion of proton resonances in all regions of the spectrum. However, the Ca(II)-saturated peptide is insoluble above 0.15 mM peptide concentration in aqueous solution over a range of pH, ionic strength, and temperature values. Previous studies on a similarly sized fragment derived from factor IX, factor IX (1−45), indicated that this peptide maintains a stable, compact Ca(II)-bound structure in the presence of 5 M urea (Medved et al., 1994). Having tested an array of solvents to enhance solubility of the factor IX (1−47)−Ca(II) complex, we found that optimal conditions employed a mixture of 3 M urea and 2.5 M

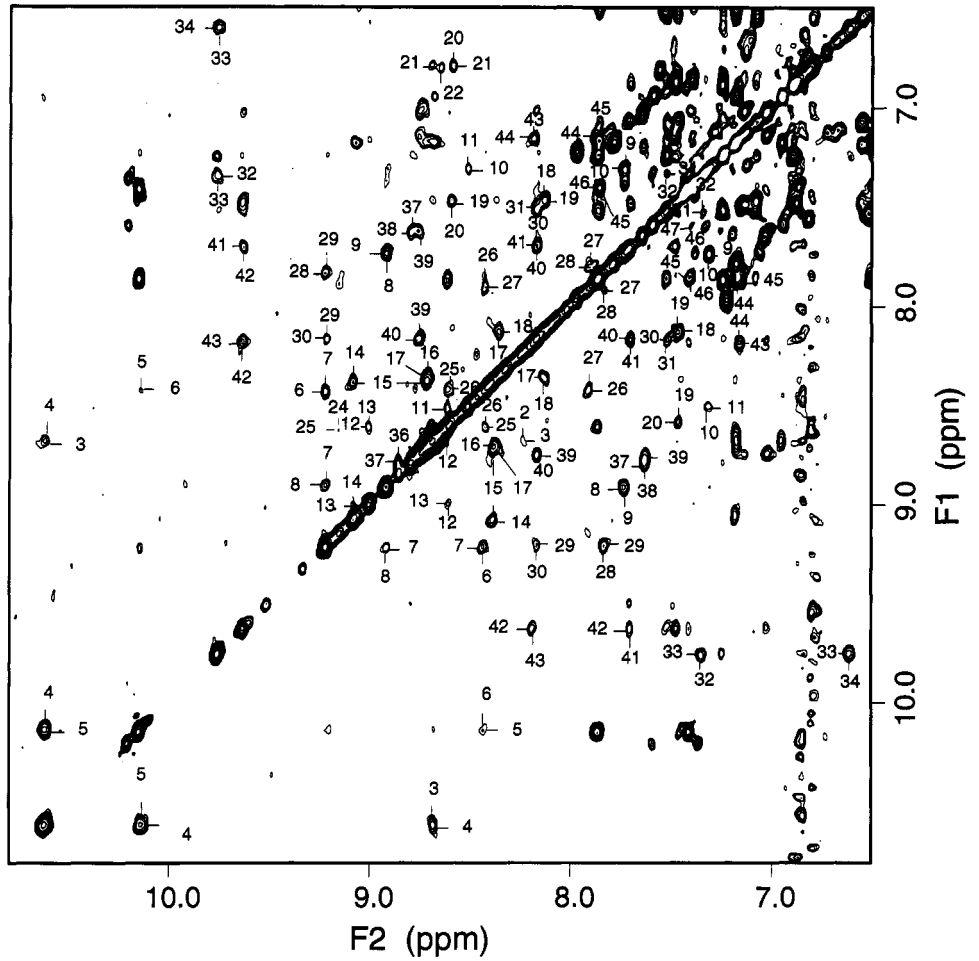

FIGURE 2: Two-dimensional ^{1}H NMR spectrum of the factor IX (1−47)−Ca(II) binary complex in the amide−amide proton region. The cross-peaks involving sequential amide protons are labeled by residue number. The experimental conditions for the NOESY experiment are described in Materials and Methods. The mixing time was 250 ms. Most of these contacts were found in the shorter mixing time NOESY as well. Since these NOE cross-peaks were well resolved, they assisted in making sequence-specific resonance assignments.

guanidine. Since the metal-free and Ca(II)-bound forms are in slow exchange (Freedman et al., 1995), the degree of saturation with $CaCl_2$ could be assessed from the spectra. In the presence of urea, guanidine, and acetate buffer, there was an increased requirement for $CaCl_2$, compared to samples lacking these reagents, to reach saturation. This finding may reflect the greater ionic strength. The latter solvent yielded NMR spectra at 25 °C that closely resembled spectra of the peptide complex in H_2O, pH 5.9, such that the average chemical shift differences of various α and amide proton resonances were 0.10 and 0.09 ppm, respectively (Table S-1). These data provide strong evidence, within experimental error, for the close similarity between the structures under these two separate conditions, since the α and amide protons of all amino acids experience an average chemical shift change of approximately 0.4 ppm from the random coil value when they are incorporated in different secondary structures (Wishart et al., 1991). The 2D spectra were also similar (see below).

Sequential assignments of all proton resonances were made using a combination of two-dimensional DQF-COSY, TOCSY, and NOESY experiments at 35 °C (Table S-2). NOESY spectra were also collected in D_2O, and at higher and lower temperatures, to uncover protons buried underneath the water resonance and to separate overlapping proton cross-peaks. The amide−amide region of the NOESY spectrum is particularly striking since sequential amide proton contacts occur for nearly 95% of the amino acids (Figure 2). Some of the missing sequential amide proton contacts may be obscured by the diagonal. The stronger sequential amide proton contacts are indicative of helical structure.

The proton chemical shift values obtained through sequential assignments were used to identify nonneighboring interresidue NOE contacts. Long-range contacts are best exemplified in the aromatic side chain−methyl proton region and the methyl−methyl proton region of the NOESY spectrum (Figure 3). The aromatic side chain−methyl proton interactions are responsible for the shifted methyl protons in the NMR spectra. In total, we identified 427 short-, medium-, and long-range NOE contacts. The strongest long-range NOE contacts of Figure 3 and other regions of the NOESY spectrum could also be identified in the factor IX (1−47)−Ca(II) peptide in H_2O. Specifically, we observed cross-peaks between Val 31 and Phe 32 with Leu 14, and Ala 28 with Thr 38. Coupling constants, $^3J_{HN\alpha}$, measured from the splitting of amide proton cross-peaks by α protons, were used to derive 19 ϕ torsion angles. Of the 38 $\chi 1$ angles determined by a measurement of $^3J_{H\alpha\beta}$ and β-proton NOE analysis, 13 are gauche/trans, 6 are trans/gauche, 2 are gauche/gauche, 13 are non-gauche/gauche, and for valine and threonines, 4 of the 6 are trans. Stereospecific assignments were used for eight residues. A total of 851 distance restraints and 57 torsion angle restraints were entered into the distance geometry program of INSIGHT II to generate

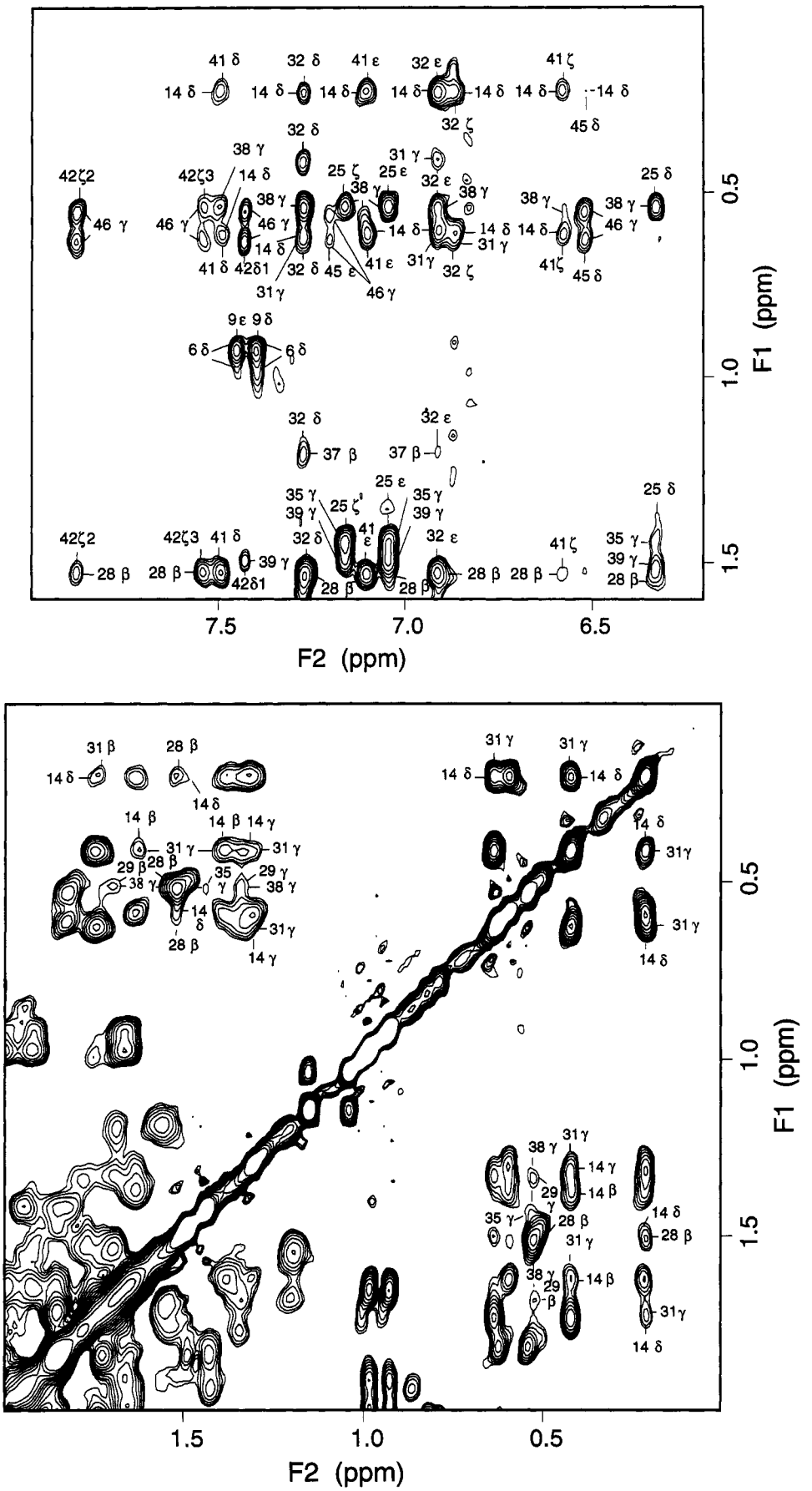

FIGURE 3: Two-dimensional ^1H NMR spectra illustrating the presence of long-range NOEs in the factor IX (1−47)−Ca(II) binary complex. (A, top) the aromatic−methyl side-chain proton region of a D_2O NOESY spectrum. (B, bottom) the methyl−methyl side-chain proton region of a NOESY spectrum. The cross-peaks are labeled by residue number and proton type. The experimental conditions for the acquisition of the NOESY spectra are described in Materials and Methods. The mixing times were 250 ms.

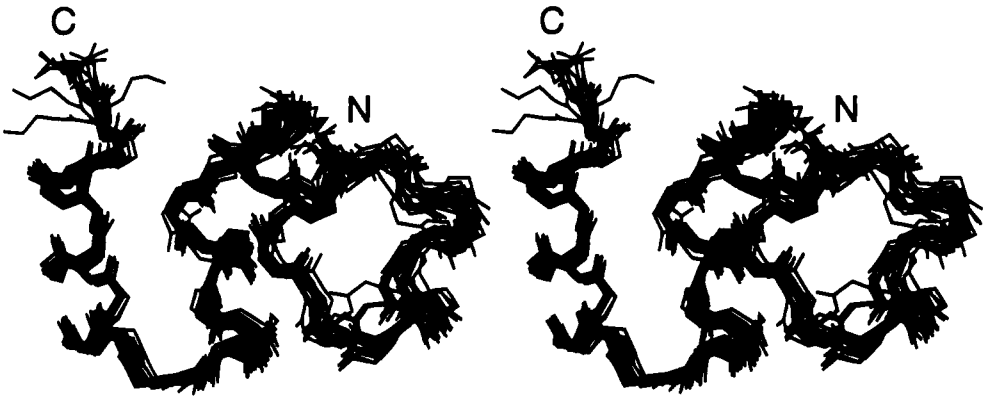

FIGURE 4: Stereoview overlay of the 17 calculated backbone structures for the factor IX (1−47)−Ca(II) binary complex. All structures are shown superimposed using the backbone atoms of the well-defined residues with the geometric average. The backbone root-mean-square deviation compared to the average is 0.6 ± 0.1 Å.

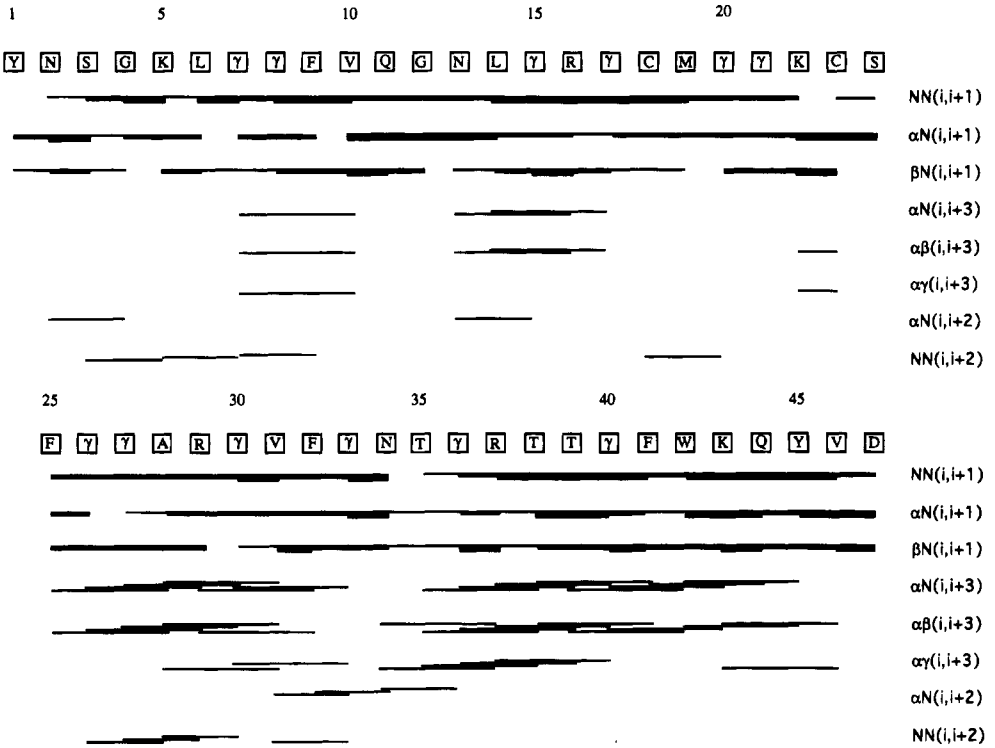

FIGURE 5: Summary of sequential and medium-range NOEs. The entire 1−47 amino acid sequence is displayed. The amino acid type and number are shown at the top of the figure in boxes. The first three lines below the sequence show (i,i+1) connectivities that were analyzed from a NOESY spectrum. A thin line indicates a weak NOE, and a thick line indicates a strong one. Medium-range NOEs typical of helical and turn structures are shown in the lower five lines.

17 final structures. No hydrogen bond constraints were employed. A comparison of these structures by superimposition of the well-defined residues with the geometric average yielded an average backbone RMSD value of 0.6 ± 0.1 Å (Figure 4) and an average RMSD for all heavy atoms (non-hydrogen atoms) of 1.1 ± 0.1 Å. The average ϕ, ψ, and χ torsion angles were measured over all structures by a vector addition method. The ϕ and ψ angles had correlations (S) near or at 1.0, except for the amino-terminal and carboxyl-terminal one or two residues, the ψ angles of residues 11 and 21, and the ϕ angles of residues 12 and 22. This indicates that the peptide backbone is almost completely ordered. In addition, correlations near or at 1.0 for 85% of the χ1 angles indicate that the side chains are also structured.

The ϕ and ψ angles have been analyzed to determine the favored backbone conformations at each residue. The majority of ϕ/ψ angles are within the right-handed helical region. Some ϕ/ψ angles are within the β-strand region but are noncontiguous in sequence, and the ϕ/ψ angle of Gla 33 is found within the unusual left-handed helical region. Consistent with the fact that glycines occupy a much larger number of energetically favorable backbone conformations, Gly 4 is also near the left-handed helical region. The torsion angles (ϕ near −60°, ψ near −50°) indicate that the dominant secondary structure is helical. Consistent with this finding is that four discrete regions within the peptide sequence have sequential and medium-range contacts typical of helices, which include sequential NH−NH, αH−NH (i,i+3), and αH−βH (i,i+3) NOE contacts (Figure 5). On the basis of both the backbone torsion angle data and NOE contact data, the following regions are helical: residues 14−17, 25−32, and 35−46. In addition, two loops in the molecule have partial helical character: (1) The disulfide loop, residues 18−23, is helical for residues 18−20, not helical for residue 23,

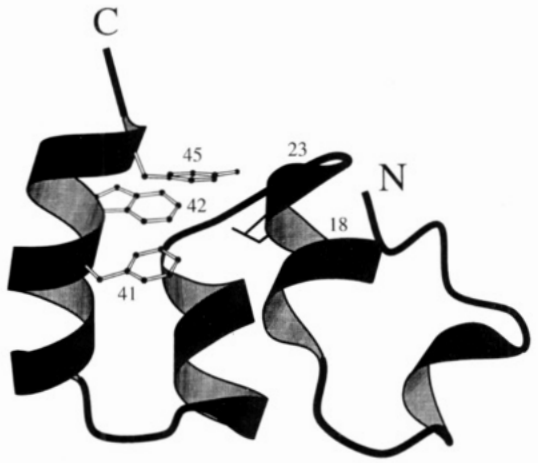

FIGURE 6: Ribbon diagram of the factor IX (1−47)−Ca(II) binary complex structure. The ribbon was generated using the program Molscript (Kraulis, 1991). The carboxyl-terminal three-quarters of the structure forms a large core composed of a significant amount of helical content. The core is adjacent to an amino-terminal loop from residues 1 to 12. The cysteines of the hexapeptide disulfide loop, residues 18 and 23, are labeled by residue number, and the disulfide bond is indicated. Only the amino-terminal half of the disulfide loop is indicated as helical, since residues 20 and 21 had poorly defined backbone torsion angles. The side chains of the conserved aromatic residues of the aromatic amino acid stack domain are displayed and labeled by residue number. The side chains face the interior of the protein near the disulfide loop and stack upon one another.

and due to poorly defined backbone angles, undetermined for residues 20 and 21. (2) A loop from residues 6−9, which is primarily defined by contacts between the side chains of Leu 6 and Phe 9, is helical for residues 7 and 8 but not for residues 6 and 9. Therefore, both these structures only approximate helices. We performed a hydrogen-bonding analysis to differentiate α helices (i,i−4 bonds) from 3_{10} helices (i,i−3 bonds) since the NOE contact data and backbone torsion angle data for helical regions (α helix, $\phi = -60°$, $\psi = -60°$; 3_{10} helix, $\phi = -60$, $\psi = -30$) were not sufficient or accurate enough to make this distinction. The 25−32 helices contain hydrogen bonds of both 3_{10} helices and α helices, the 35−46 helices are of the α-helical type, and the 6−9 and 14−20 helices could not be classified since no hydrogen bonds were consistently observed. Other than helices and random coil structure, there exist two tight four-residue turns. One tight turn is composed of residues 32 (last residue of the 25−32 helix), 33, 34, and 35 (first residue of the 35−46 helix) and is best classified as a type V′ turn ($\phi_2 \approx +80°$, $\psi_2 \approx -80°$, $\phi_3 \approx -80°$, $\psi_3 \approx +80°$) (Richardson, 1981). Another turn from residues 7−10 overlaps with the partially helical 6−9 loop and is best classified as a type I turn ($\phi_2 \approx -60°$, $\psi_2 \approx -30°$, $\phi_3 \approx -90°$, $\psi_3 \approx 0°$) (Richardson, 1981). In the segment of residues 6−10 the sequential and medium range NOE contact data displayed in Figure 5 show features of both helices and type I turns. Common to four-residue turns, a hydrogen bond is present between the amide proton donor of residue 10 and the carbonyl oxygen acceptor of residue 7.

The tertiary structure consists of a large carboxyl-terminal globular core (residues 13−47) adjacent to a large amino-terminal loop (residues 1−12) (Figure 6). The core of the protein consists of three helical segments (residues 14−17, 25−32, and 35−46) in which the first and second helices are separated by the disulfide loop (residues 18−23), itself resembling a helical turn, and the second and third helices are separated by a reverse hairpin turn (residues 32−35). The large amino-terminal loop contains the two overlapping turn structures from residues 6−10, and the partial helical character of the 6−9 turn is indicated by helical ribbon in Figure 6. Tyr 1 closes the amino-terminal loop by coming in close proximity to the disulfide loop as demonstrated by NOE contacts between Tyr 1 and residues 21−24. Despite these contacts with the core of the protein, the Tyr 1 aromatic ring is not buried (Figure 7); however, the position of the free amino group with respect to the rest of the peptide cannot be accurately determined due to a poorly defined ψ angle. The position of the large amino-terminal loop is established in relation to the core of the protein by NOE contacts between Gla 7 and Val 10 with Arg 16. The carboxyl-terminal α helix contains three aromatic amino acids (Phe 41, Trp 42, and Tyr 45) that are strictly conserved among the vitamin K-dependent blood clotting proteins. The aromatic rings stack upon one another and face the protein interior adjacent to the disulfide loop (Figure 6). Thus, the amino and carboxyl termini of the molecule form a "sandwich" with the disulfide loop to form a compact tertiary structure.

Factor IX contains 12 Gla residues at sequence positions 7, 8, 15, 17, 20, 21, 26, 27, 30, 33, 36, and 40. The dicarboxylic acid side chains of the first nine Gla residues, which are conserved in all vitamin K-dependent blood clotting and regulatory proteins, are mostly clustered within the interior of the molecule (Figure 8). They enclose a negatively charged space between the amino-terminal loop and the core of the protein. The carboxyl-terminal three Gla residues, including Gla 33, Gla 36, and Gla 40, project into the solvent-exposed exterior. On the surface of the carboxyl-terminal α helix, Gla 40 is interposed between two cationic residues, Arg 37 and Lys 43.

The position of the bound calcium ions cannot be directly determined by ^{1}H NMR spectroscopy. To determine whether the internal carboxylate space in factor IX could accommodate the Ca(II) cluster observed in bovine prothrombin fragment 1 (Soriano-Garcia et al., 1992), 20 additional structures were calculated using the intercalcium ion distances and distances between the α, β, and γ carbons of Gla residues and liganded calcium ions defined by the prothrombin fragment 1−Ca(II) crystal structure. We found that these restraints further constrained our structure (i.e., the average backbone RMSD by superimposition with the geometric average is 0.5 ± 0.1 Å, and the average RMSD of all heavy atoms is 1.0 ± 0.1 Å), but the backbone conformation remained essentially the same (Figure 9). The latter fact is based on the finding that the average ϕ and ψ angle differences at each residue for the structures calculated in the presence and absence of Ca(II) distance restraints are generally smaller than 10°, and only a few approach 30°. This is further supported from the superposition of the average structures from each set of structures, in which a backbone RMSD of 0.5 Å was calculated. Thus, the Ca(II) cluster of bovine prothrombin fragment 1 was able to fit the human factor IX peptide structure.

The majority of hydrophobic residues are found within the carboxyl-terminal core and are involved in hydrophobic packing interactions which stabilize this region in the Gla domain (Figure 7). There is little hydrophobic surface exposed to solvent in this region. In contrast, a small

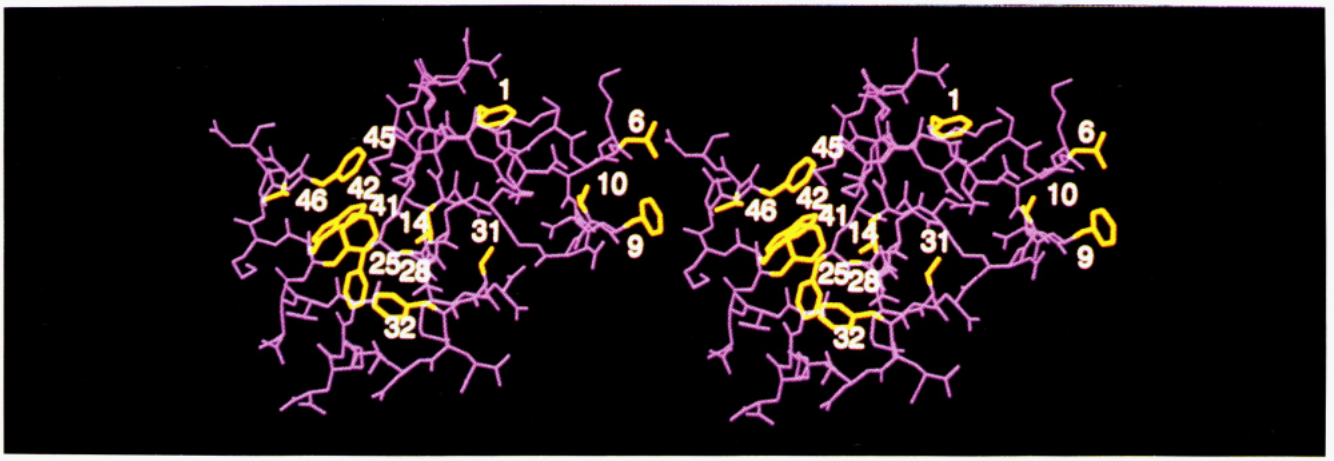

FIGURE 7: Stereoview of the factor IX (1−47)−Ca(II) structure indicating the location of the hydrophobic residues. The lowest energy structure is shown. The hydrophobic residue side chains are displayed in yellow and labeled by residue number. The majority of the hydrophobic side chains are in the carboxyl-terminal region of the molecule and are directed internally. Three residues in the amino-terminal region, Leu 6, Phe 9, and Val 10, are exposed to solvent and form a hydrophobic surface patch. The aromatic ring of Tyr 1 is found at the surface of the protein and makes contacts about the disulfide loop.

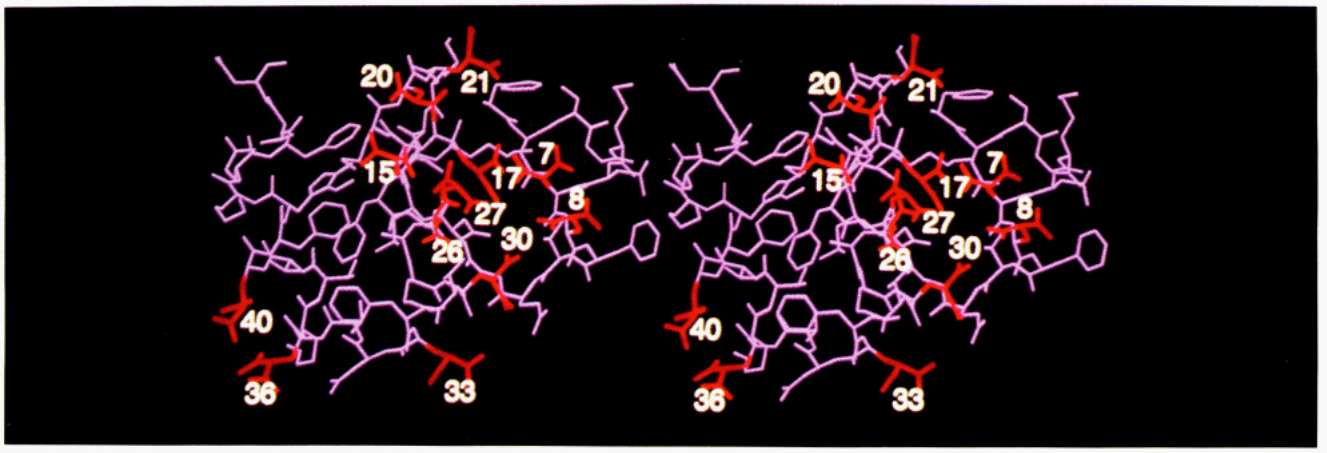

FIGURE 8: Stereoview of the factor IX (1−47)−Ca(II) structure indicating the location of the Gla residues. The lowest energy structure is shown. The 12 Gla residue side chains are displayed in red and labeled by residue number. The amino-terminal 9 Gla residues are mainly directed toward the protein interior and create a negatively charged internal space. The carboxyl-terminal three Gla residues face the solvent.

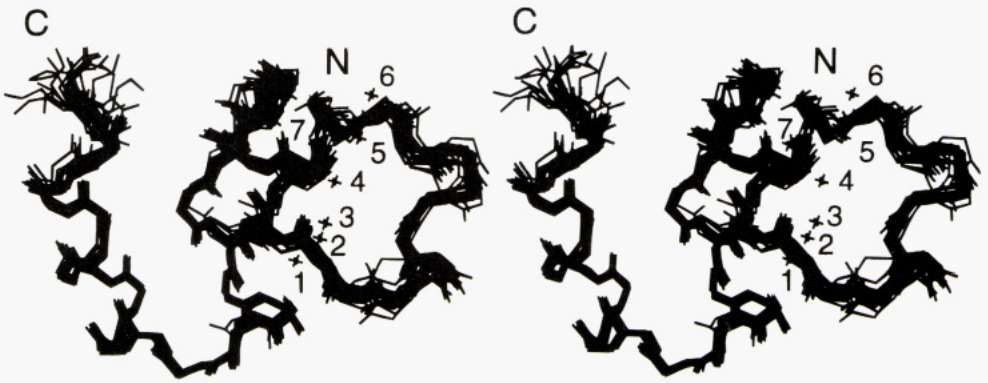

FIGURE 9: Stereoview overlay of the 20 backbone structures for the factor IX (1−47)−Ca(II) binary complex that were calculated using the Ca(II) distance restraints of the prothrombin fragment 1−Ca(II) crystal structure. All structures are shown superimposed using the backbone atoms of the well-defined residues with the geometric average. The structures were calculated using the experimental data (used to derive the structures of Figure 4) plus additional restraints provided by the inter-calcium ion and Gla residue-to-calcium ion distances as defined by the crystal structure of prothrombin fragment 1 (Soriano-Garcia et al., 1992). The seven calcium ions of only the lowest energy structure are shown for simplicity of illustration. The backbone root-mean-square deviation compared to the average is 0.5 ± 0.1 Å.

hydrophobic patch in the amino-terminal loop consisting of Leu 6, Phe 9, and Val 10 faces the solvent. Numerous interproton NOE contacts between Leu 6 and Phe 9 and between Gla 7 and Val 10 define the three-dimensional structure of this surface patch.

DISCUSSION

Since the discovery of γ-carboxyglutamic acid in 1974 (Stenflo et al., 1974; Nelsestuen et al., 1974) considerable effort has been expended to describe the metal and phos-

pholipid binding properties of vitamin K-dependent blood coagulation proteins [for review, see Furie and Furie (1988)]. The Ca(II)-mediated structural changes in the Gla domain that lead to the formation of a phospholipid binding site have been probed using low-resolution techniques such as fluorescence quenching, circular dichroism, and conformation-specific antibodies (Nelsestuen, 1976; Bloom & Mann, 1978; Furie et al., 1978; Borowski et al., 1986). Only recently has the first three-dimensional structure of a Ca(II)-bound Gla domain been determined, the crystal structure of Ca(II)-stabilized bovine prothrombin fragment 1 (Soriano-Garcia et al., 1992). X-ray crystallography and NMR methods have also been applied to other coagulation protein domains [for review, see Stubbs and Bode (1994)] but 2D NMR methods have not been applied to problems related to Gla domain structure and function.

A small synthetic analog of factor IX, the factor IX (1−47) peptide, has been used to study the Ca(II)-stabilized structure of factor IX since its size and efficient production make it amenable to analysis by NMR spectroscopy, and it expresses the metal and phospholipid binding properties characteristic of human factor IX (Jacobs et al., 1994). In the first stage of this study, we described the NMR-derived structure of the metal-free form of factor IX (1−47) (Freedman et al., 1995), a structure that does not bind phospholipid membranes. The relative disorder of this structure compared to the Ca(II)-bound prothrombin fragment I crystal structure suggested that additional structure was required for the phospholipid binding function of factor IX. In this report we have described the solution structure of the factor IX (1−47)−Ca(II) binary complex.

The vitamin K-dependent blood coagulation proteins and their Gla-containing fragments aggregate in the presence of calcium ions and at high protein concentration. Although factor IX (1−47), like factor IX, is soluble at the physiologic concentrations of factor IX (~0.09 μM) and up to about 0.15 mM, the higher concentrations required for efficient collection of NMR data were not achievable at saturating concentrations of calcium ions. Alterations in pH, ionic strength, and temperature were not effective in promoting a stable, soluble peptide. We found that in 3 M urea/2.5 M guanidine, the peptide at 1.5−2.1 mM concentration and 120 mM $CaCl_2$ remained in solution and maintained its native structure. This conclusion is based on the similarity between 1D and 2D spectra acquired from the Ca(II)-bound peptide with and without the guanidine/urea. The preservation of a native Gla domain structure with these agents is consistent with a previous report on a fragment of factor IX consisting of residues 1−45 (Medved et al., 1994). This group found that the Ca(II)-bound peptide had a stable compact structure in 5 M urea. In the absence of urea, the Ca(II)-bound peptide self-associated. Thus, the primary effect of these solubilization conditions is to disrupt aggregation without denaturation. In this respect, we have no evidence for intermolecular association from our analysis of NOE contacts in the NOESY spectrum. There are other precedents for polypeptides that maintain stable structures under these conditions. For instance, the structure of bovine pancreatic trypsin inhibitor (BPTI) remains native in 8 M urea (Liepinsh & Otting, 1994). For BPTI the presence of disulfide bonds probably contributes significantly to this stability, and likewise in our peptide the single disulfide may also contribute to its stability. Prior to completion of the Ca(II)-bound factor IX (1−47) NMR structure, the structure of apo-factor IX (1−47) was compared to the analogous region of the prothrombin fragment I−Ca(II) crystal structure (Freedman et al., 1995). Apo-factor IX (1−47) contains three discrete regions of secondary structure in common with prothrombin fragment 1−Ca(II) (residues 6−9, 18−23, and 37−46). In the factor IX apopeptide, the intervening regions are unstructured. We can now compare the apo- and Ca(II)-bound factor IX (1−47) structures. The three structured segments in the apopeptide are also conserved in the factor IX (1−47)−Ca(II) structure with an average RMSD of ~1 Å for each segment (data not shown). However, the loop from residues 6 to 9 more closely approximates a helix in the Ca(II)-bound peptide based on the ϕ and ψ angle values, which are helical for residues 7 and 8. In addition, the conformation of the tryptophan 42 side chain differs between the two structures (Figure 10). There is an 87° and 32° reorientation of the $\chi 1$ and $\chi 2$ angles, respectively. Moreover, the $\chi 1$ rotameric conformation changes from gauche/gauche to gauche/trans following the binding of Ca(II).

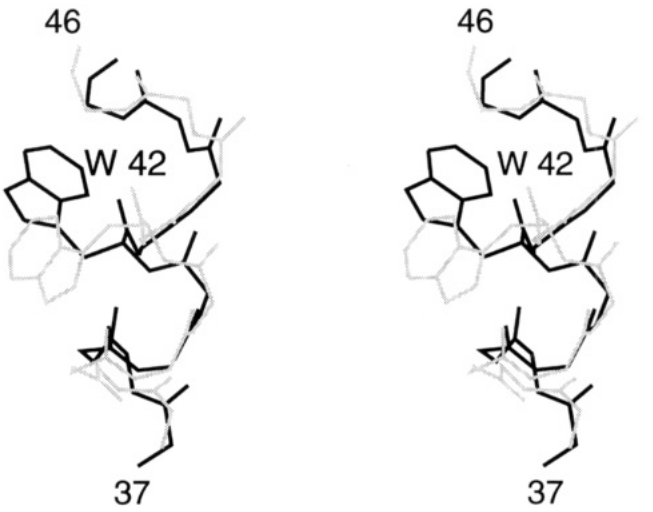

FIGURE 10: The Ca(II)-induced reorientation of the Trp 42 indole ring. Stereoview overlay of the α-helical region, residues 37−46, of apo-factor IX (1−47) shown in gray with the analogous region of the factor IX (1−47)−Ca(II) binary complex shown in black. The $\chi 1$ and $\chi 2$ angle differences for Trp 42 are 87° and 32°, respectively, indicating the conformational change upon Ca(II) binding.

There are several important differences between the apo structure and Ca(II)-bound structure of factor IX (1−47). First, the Ca(II)-bound factor IX (1−47) structure has an increased amount of helical content relative to the apo structure. This was initially inferred from a comparison of the amide−amide region of the NOESY spectra (Freedman et al., 1995). There is an abundance of sequential amide contacts for most of the Ca(II)−peptide sequence. These include some $i > i+2$ contacts. In contrast, sequential amide contacts in the apopeptide are confined to the three short regions of defined structure, residues 6−9, 18−23, and 37−46. Detailed analysis of the factor IX (1−47)−Ca(II) structure reveals that compared to the apo structure there are four to five additional helical turns throughout the Ca(II)−peptide structure. These results are consistent with the Ca(II)-induced increase in helical content in a factor IX Gla domain peptide as monitored by circular dichroism (Vysotchin et al., 1993). The interhelical regions are composed of structured loops and turns which are unstructured in the apopeptide, aside from the disulfide loop (residues 18−23).

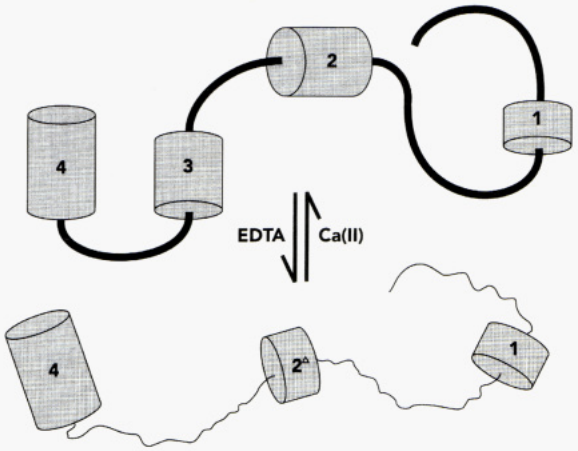

FIGURE 11: Model of the Ca(II)-induced conformational transition in factor IX (1−47) as determined by NMR. In the absence of metal ions, the factor IX (1−47) peptide is generally unstructured except for the presence of three well-ordered regions, residues 6−9 (cylinder 1), 18−23 (cylinder 2^), and 37−46 (cylinder 4). Following Ca(II) binding these three regions fold into a well-ordered tertiary structure containing additional helical regions, including residues 25−32 (cylinder 3) and residues 14−17 (amino-terminal part of cylinder 2), that are separated by structured loops and turns. The disulfide loop resembles a helical turn, and when preceded by the 14−17 helix, they together form a continual two-turn helix. The Ca(II)-bound conformer binds phospholipids.

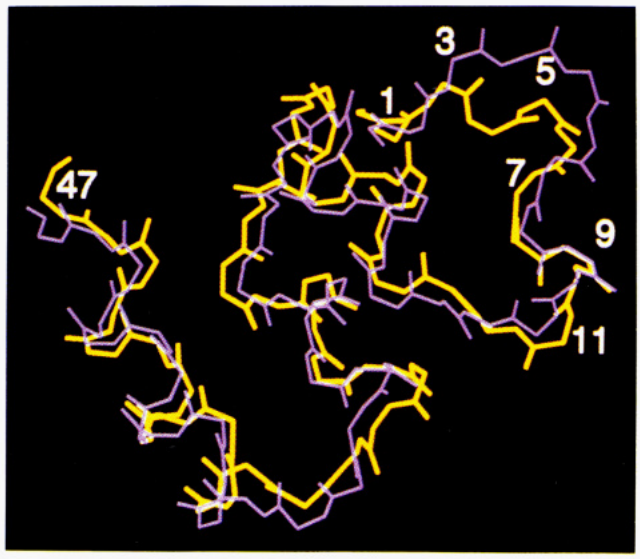

FIGURE 12: Overlay of the factor IX (1−47)−Ca(II) NMR structure with the analogous region of the prothrombin fragment 1−Ca(II) crystal structure. Factor IX (1−47) is shown in yellow and prothrombin (1−47) in purple. The lowest energy factor IX (1−47)−Ca(II) structure was used for superimposition. The backbone structures are strikingly similar from residues 12 to 47 (RMSD is approximately 1.3 Å). However, the backbone conformation deviates in the 1−11 residue region (labeled by residue number). A significant conformational difference is observed between residues 3 and 6.

Second, the Ca(II)-bound peptide is a compact tertiary structure defined by long-range NOEs that do not exist in the apopeptide NOESY spectra. Some of the large Ca(II)-induced chemical shift changes can now be explained from our three-dimensional model. Most of the aliphatic residue methyl protons are shifted by interacting aromatic groups. The amide protons of Gla 21 [apo, 8.55 ppm; Ca(II), 6.80 ppm] and Asn 34 [apo, 8.34 ppm; Ca(II), 6.61 ppm] are significantly shifted upfield by interaction with the aromatic rings of Tyr 1 and Phe 32, respectively. The α protons of Asn 2 [apo, 4.71 ppm; Ca(II), 5.19 ppm], Cys 18 [apo, 4.70 ppm; Ca(II), 5.35 ppm], Met 19 [apo, 4.50 ppm; Ca(II), 5.30 ppm], Cys 23 [apo, 4.64 ppm; Ca(II), 5.88 ppm], and Ser 24 [apo, 4.38 ppm; Ca(II), 5.06 ppm] are shifted downfield (to between 5 and 6 ppm) by the aromatic rings of Tyr 1 (for residues 2 and 23), Tyr 45 (for residues 18 and 19), and Trp 42 (for residue 24). The ϵ-amino group of Arg 16 [apo, 7.19 ppm; Ca(II), 8.32 ppm] is likely shifted downfield by an interaction with the carboxylate group of Gla 7, whereas the ϵ-amino group of Arg 29 [apo, 7.25 ppm; Ca(II), 8.73 ppm] is shifted downfield by an interaction with the aromatic ring of Phe 25. Third, the side-chain conformation of Trp 42 differs substantially between the apopeptide structure and Ca(II)-bound structure. Similar results were reported for prothrombin (Soriano-Garcia et al., 1992). Therefore, intrinsic tryptophan fluorescence quenching upon addition of Ca(II) to factor IX occurs as a result of burial of Trp 42 adjacent to the disulfide loop and reorientation of the indole ring. The conformational transition between the apo- and Ca(II)-bound factor IX (1−47) structures is shown diagrammatically in Figure 11. The three independent, structured regions of the apopeptide fold reversibly into a compact Ca(II)-bound tertiary structure with increased helical content. The increased order and secondary structure of the Ca(II)-bound peptide are necessary for phospholipid binding.

A structural comparison can be made between the factor IX (1−47)−Ca(II) solution structure and the analogous region of the prothrombin fragment 1−Ca(II) crystal structure (Soriano-Garcia et al., 1992). Figure 12 shows an overlay of the two backbone structures. The initial impression is that the global fold of each protein is strikingly similar, particularly from residues 12 to 47 (RMSD is ~1.3 Å). However, the backbone conformations deviate in the first 11 residues and most prominently between residues 3 and 6. This is evident from the ϕ angle values of these latter residues. The ϕ angle of residue 4 is positive in factor IX (84°) and negative in prothrombin (−120°), and the ϕ angles of residues 5 and 6 are negative in factor IX (−99°, −126°) and positive in prothrombin (175°, 74°). There are three possibilities for this observed conformational difference. First, this may represent a true difference in conformation between the native proteins. It is known through mutagenesis studies that Gla residues at identical positions in vitamin K-dependent proteins play different roles (Zhang et al., 1992; Ratcliffe et al., 1993). In addition, the phospholipid binding affinity and specificity vary among vitamin K-dependent proteins (Mann et al., 1990). Therefore, differences in structure may reflect differences in function. Second, in this region of the prothrombin fragment 1 crystal structure, residues 4 and 5 were associated with poor electron density, and thus, the certainty of the structure derived from the electron density map in this region is diminished (Soriano-Garcia et al., 1992). Furthermore, distortions may occur at the crystal packing interface. In this regard, intermolecular van der Waals interactions involving residues 5 and 6 were reported between adjacent molecules. Third, the solvent system used to determine the factor IX (1−47)−Ca(II) structure may affect this region of the peptide. However, the chemical shifts and NOE contacts in this region are similar, within experimental error, to the Ca(II)−peptide in the absence of solubilizing agents. In sum, it is not clear whether the conformational difference at the amino terminus between prothrombin and factor IX is significant and must

await further study of the prothrombin peptide by NMR spectroscopy.

The amino termini of vitamin K-dependent proteins are protected from chemical modification in the presence but not the absence of calcium ions (Welsch & Nelsestuen, 1988; Schwalbe et al., 1989). Conversely, chemical modification of the amino termini in the absence of Ca(II) abolishes phospholipid binding in the presence of calcium ions. Therefore, a free amino terminus is required for normal Gla domain function. The crystal structure of prothrombin fragment 1−Ca(II) (Soriano-Garcia et al., 1992) revealed that the amino-terminal Ala 1 becomes completely buried within the protein interior. The only known modification of the amino terminus that does not affect phospholipid binding is trinitrophenylation. Soriano-Garcia et al. (1992) postulated that this modification leads to an alternative conformation of the amino-terminal region in order to support normal function, since such a bulky group could not be accommodated by the space occupied by Ala 1. Factor IX is the only known vitamin K-dependent protein to contain an amino-terminal tyrosine. This bulky side chain is similar in size to trinitrophenylated Ala 1 in prothrombin. We find that the aromatic ring of Tyr 1 is not buried within the interior of the protein, although this residue makes some of the close interresidue contacts seen for Ala 1 in prothrombin. Since the first few residues that follow Tyr 1 have a different backbone conformation compared to prothrombin, this bulky residue may produce the alternative conformation that occurs in trinitrophenylated prothrombin.

The factor IX Gla domain contains 12 Gla residues, of which the first 11 are highly conserved in vitamin K-dependent proteins. In contrast, prothrombin only contains 10 Gla residues. The presence of internal metal binding sites in prothrombin was originally proposed on the basis of NMR paramagnetic relaxation studies (Furie et al., 1979). In the recent crystallographic analysis, prothrombin fragment 1 Gla residue dicarboxylic acid side chains, except for that of Gla 33, were found to point to the interior of the folded protein (Soriano-Garcia et al., 1992). Gla 33 is the only Gla residue not involved in binding calcium ions, and no electron density was observed for the side chain. All the Gla residues as far as the γ carbon are formally defined structurally in the factor IX (1−47)−Ca(II) solution structure. Similar to prothrombin, many of the carboxyl groups of the amino-terminal nine Gla residues are also directed to the protein interior, thereby confirming the results found for prothrombin. The three carboxyl-terminal Gla residues are exposed to solvent, and their role, if any, in Ca(II) binding is unknown. The carboxyl-terminal Gla residue, Gla 40, may be required to stabilize the carboxyl-terminal α helix through ionic interactions since the $i+3$ and $i-3$ residues are basic and found on the same side of the α helix. In prothrombin, residues 37, 40, and 43 are alanine residues, but this amino acid is well recognized to preserve secondary structure (Cunningham & Wells, 1989). To determine if the negatively charged space within the protein interior formed by the first nine Gla residues in factor IX could accommodate the four buried calcium ions found in prothrombin, we performed structure calculations that included the Ca(II) distance restraints defined by the prothrombin fragment 1 crystal structure (Soriano-Garcia et al., 1992). We found that inclusion of these restraints refined the quality of our structure but did not modify the backbone conformation, showing that the calcium ions of prothrombin can be accommodated by the Factor IX structure.

The majority of hydrophobic residues are found within the interior of the carboxyl-terminal three-quarters of the factor IX (1−47)−Ca(II) structure. Three hydrophobic residues in the amino-terminal loop, Leu 6, Phe 9, and Val 10, form a hydrophobic surface patch. These residues are also found within a structured loop in the apopeptide. The same hydrophobic surface patch is found in prothrombin, but positions 9 and 10 are substituted with valine and arginine, respectively (Soriano-Garcia et al., 1992). Leu 6 is a highly conserved amino acid in the vitamin K-dependent proteins. Recently, this residue was found to contribute to the phospholipid binding energy of protein C, and it has been hypothesized that this residue plays a central role in phospholipid binding by all vitamin K-dependent proteins (Zhang & Castellino, 1994). These results are consistent with a hydrophobic component of the phospholipid binding energy in vitamin K-dependent proteins (Atkins & Ganz, 1992). In turn, we postulate that the hydrophobic component responsible for phospholipid binding in factor IX includes residues 6−10 since this hydrophobic region is the most solvent-exposed and, thus, is readily accessible to interaction with phospholipid membranes. Comparison of the structure of the factor (1−47)−Ca(II) binary complex with the structure of the factor IX (1−47)−Mg(II) binary complex should reveal the phospholipid binding site since the former structure is associated with phospholipid binding while the latter structure does not bind phospholipid membranes.

ACKNOWLEDGMENT

We thank Margaret Jacobs for synthesizing the factor IX (1−47) peptide.

SUPPORTING INFORMATION AVAILABLE

Table S-1 describing the chemical shift differences between factor IX (1−47)−Ca(II) in H_2O and factor IX (1−47)−Ca(II) in GnHCl/urea solution and Table S-2 containing the proton resonance assignments for the factor IX (1−47)−Ca(II) peptide (3 pages). Ordering information is given on any current masthead page.

REFERENCES

Amphlett, G. W., Kisiel, W., & Castellino, F. J. (1981) *Biochemistry 20*, 2156−2161.

Atkins, J. S., & Ganz, P. R. (1992) *Mol. Cell. Biochem. 112*, 61−71.

Bajaj, P. S. (1982) *J. Biol. Chem. 257*, 4127−4132.

Bax, A., & Davis, D. G. (1985) *J. Magn. Reson. 65*, 355−360.

Bloom, J. W., & Mann, K. G. (1978) *Biochemistry 17*, 4430−4438.

Borowski, M., Furie, B. C., Bauminger, S., & Furie, B. (1986) *J. Biol. Chem. 261*, 14969−14975.

Cunningham, B. C., & Wells, J. A. (1989) *Science 244*, 1081−1085.

Detlefsen, D. J., Thanabal, V., Pecoraro, V. L., & Wagner, G. (1991) *Biochemistry 30*, 9040−9046.

Driscoll, P. C., Clore, G. M., Beress, L., & Gronenborn, A. M. (1989) *Biochemistry 28*, 2178−2187.

Freedman, S. J., Furie, B. C., Furie, B., & Baleja, J. D. (1995) *J. Biol. Chem. 270*, 7980−7987.

Furie, B., & Furie, B. C. (1988) *Cell 53*, 505−518.

Furie, B., Provost, K. L., Blanchard, R. A., & Furie, B. C. (1978) *J. Biol. Chem. 253*, 8980−8987.

Furie, B. C., & Furie, B. (1975) *J. Biol. Chem. 250*, 601−608.

Furie, B. C., Blumenstein, M., & Furie, B. (1979) *J. Biol. Chem. 254*, 12521−12530.
Havel, T. F. (1991) *Prog. Biophys. Mol. Biol. 56*, 43−78.
Hyberts, G., Märki, W., & Wagner, G. (1987) *Eur. J. Biochem. 164*, 625−635.
Hyberts, S. G., Goldberg, M. S., Havel, T. F., & Wagner, G. (1992) *Protein Sci. 1*, 736−751.
Jacobs, M., Freedman, S. J., Furie, B. C., & Furie, B. (1994) *J. Biol. Chem. 269*, 25494−25501.
Kraulis, P. J. (1991) *J. Appl. Crystallogr. 24*, 946−950.
Liebman, H. A., Furie, B. C., & Furie, B. (1987) *J. Biol. Chem. 262*, 7605−7612.
Liepinsh, E., & Otting, G. (1994) *J. Am. Chem. Soc. 116*, 9070−9074.
Ludvigsen, S., & Poulsen, F. M. (1992) *J. Biomol. NMR 2*, 227−233.
Mann, K. G., Nesheim, M. E., Church, W. R., Haley, P., & Krishnaswamy, S. (1990) *Blood 76*, 1−16.
Medved, L., Vysotchin, A., & Ingham, K. C. (1994) *Biochemistry 33*, 478−485.
Nelsestuen, G. L. (1976) *J. Biol. Chem. 251*, 5648−5656.
Nelsestuen, G. L., & Suttie, J. W. (1972) *Biochemistry 11*, 4961−4964.
Nelsestuen, G. L., Zytkovicz, T. H., & Howard, J. B. (1974) *J. Biol. Chem. 249*, 6347−6350.
Nelsestuen, G. L., Broderius, M., & Martin, G. (1976) *J. Biol. Chem. 251*, 6886−6893.
Pardi, A., Billeter, M., & Wüthrich, K. (1984) *J. Mol. Biol. 180*, 741−751.
Ratcliffe, J. V., Furie, B., & Furie, B. C. (1993) *J. Biol. Chem. 268*, 24339−24345.
Richardson, J. S. (1981) *Adv. Protein Chem. 34*, 167−339.
Schwalbe, R. A., Ryan, J., Stern, D. M., Kisiel, W., Dahlbäck, B., & Nelsestuen, G. L. (1989) *J. Biol. Chem. 264*, 20288−20296.
Soriano-Garcia, M., Padmanabhan, K., de Vos, A. M., & Tulinsky, A. (1992) *Biochemistry 31*, 2554−2566.
Stenflo, J., Fernlund, P., Egan, W., & Roepstorff, P. (1974) *Proc. Natl. Acad. Sci. U.S.A. 71*, 2730−2733.
Strickland, D., & Castellino, F. J., (1980) *Arch. Biochem. Biophys. 199*, 61−66.
Stubbs, M. T., & Bode, W. (1994) *Curr. Opin. Struct. Biol. 4*, 823−832.
Vysotchin, A., Medved, L. V., & Ingham, K. C. (1993) *J. Biol. Chem. 268*, 8436−8446.
Welsch, D. J., & Nelsestuen, G. L. (1988) *Biochemistry 27*, 4939−4945.
Wishart, D. S., Sykes, B. D., & Richards, F. M. (1991) *J. Mol. Biol. 222*, 311−333.
Wüthrich, K. (1986) *NMR of Proteins and Nucleic Acids*, John Wiley & Sons, Inc., New York.
Wüthrich, K. (1989) *Science 243*, 45−50.
Wüthrich, K., Wider, G., Wagner, G., & Braun, W. (1982) *J. Mol. Biol. 155*, 311−319.
Zhang, L., & Castellino, F. J. (1994) *J. Biol. Chem. 269*, 3590−3595.
Zhang, L., Jhingan, A., & Castellino, F. J. (1992) *Blood 80*, 942−952.

BI9509053